

# Efficient GANs for Document Image Binarization Based on DWT and Normalization

Rui-Yang Ju<sup>1</sup>, KokSheik Wong<sup>2</sup>, and Jen-Shiun Chiang<sup>3</sup>

<sup>1</sup> National Taiwan University, Taipei City, Taiwan  
jryjry1094791442@gmail.com

<sup>2</sup> Monash University, Kuala Lumpur, Malaysia  
wong.koksheik@monash.edu

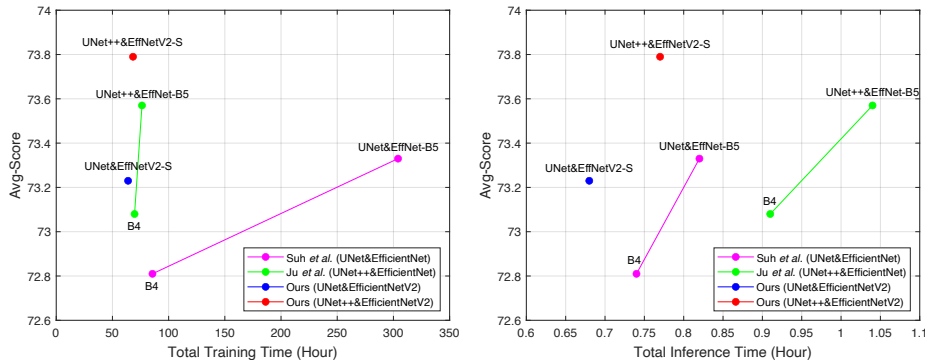
<sup>3</sup> Tamkang University, New Taipei City, Taiwan  
jsken.chiang@gmail.com

**Abstract.** For document image binarization task, generative adversarial networks (GANs) can generate images where shadows and noise are effectively removed, which allow for text information extraction. The current state-of-the-art (SOTA) method proposes a three-stage network architecture that utilizes six GANs. Despite its excellent model performance, the SOTA network architecture requires long training and inference times. To overcome this problem, this work introduces an efficient GAN method based on the three-stage network architecture that incorporates the Discrete Wavelet Transformation and normalization to reduce the input image size, which in turns, decrease both training and inference times. In addition, this work presents novel generators, discriminators, and loss functions to improve the model’s performance. Experimental results show that the proposed method reduces the training time by 10% and the inference time by 26% when compared to the SOTA method while maintaining the model performance at 73.79 of Avg-Score. Our implementation code is available on GitHub at [https://github.com/RuiyangJu/Efficient\\_Document\\_Image\\_Binarization](https://github.com/RuiyangJu/Efficient_Document_Image_Binarization).

**Keywords:** Document image processing · Document image enhancement · Document image binarization · Image generation · Generative adversarial networks · Discrete wavelet transformation

## 1 Introduction

Document image binarization has an important position in document image analysis and recognition [34], as it significantly impacts subsequently stages of the recognition process and layout analysis. Ancient documents often suffer from various types of degradation, including paper yellowing, text fading, and page bleeding [13, 19, 41], which further complicate the binarization process. For badly degraded documents, traditional image processing methods [23, 25, 36] are poor



Method	Model	Avg $\uparrow$	Total Train $\downarrow$	Total Infer $\downarrow$
Suh <i>et al.</i> [40]	UNet&EffNet-B5	73.33	304.12h	0.82h
Ju <i>et al.</i> [16]	UNet++&EffNet-B5	73.57	76.29h	1.04h
<b>Ours</b>	UNet&EffNetV2-S	73.23	63.91h	<b>0.68h</b>
<b>Ours</b>	UNet++&EffNetV2-S	<b>73.79</b>	<b>68.43h</b>	0.77h

**Fig. 1:** Graphs of Avg-Score vs. Total Training and Inference Times (measured on (H)-DIBCO Datasets using NVIDIA GeForce RTX 4090 GPUs).

at eliminating shadows and noise, and even lose text information. Therefore, researchers are appealing to deep learning-based methods, and some have achieved satisfactory results [17, 20, 38].

For instance, Souibgui *et al.* [37] introduce a novel encoder-decoder architecture based on Vision Transformer (ViT), which achieves good performance on the H-DIBCO 2018 [31] dataset. Yang *et al.* [46] propose an end-to-end gated convolutions-based network (GDB) to address the challenge of inaccurate stroke edge extraction in documents, and achieves the state-of-the-art (SOTA) performance on the H-DIBCO 2014 [24] and DIBCO 2017 [33] datasets. To improve the performance of the model, these methods employ the “leave-one-out” strategy to construct the training set (viz., for the selected test set, all the remaining datasets are used to train the model). Considering the computing resources for model training, we believe that the strategy [12, 16, 40, 45] of fixed training set is more efficient compared to the “leave-one-out” strategy, where the SOTA methods for such strategy are Suh *et al.* [40] and Ju *et al.* [16].

Although Suh *et al.*’s method [40] and Ju *et al.*’s method [16] achieve excellent performances on several benchmark datasets, the time needed for training and inferencing are too long due to the use of six generative adversarial networks (GANs) [9]. To address this problem, we propose an efficient GAN method for document image binarization that significantly reduces both the training and inference times while maintaining the model performance (FM, p-FM, and Avg), and the results are summarized in Fig. 1. Our contributions are as follows:

- Proposes a novel method to reduce both the training and inference times of GANs by employing discrete wavelet transformation (DWT) and normalization to decrease the size of the input image;
- Improves the SOTA methods through the design of novel generators, discriminators, and loss functions. These improvements make the proposed method more efficient for document image binarization;
- Outperforms the SOTA methods in terms of the model performance (FM, p-FM, and Avg), training and inference times for seven benchmark datasets.

The rest of this paper is organized as follows: Section 2 introduces the application of semantic segmentation and image generation networks to document image binarization task, and reviews the SOTA methods for document image binarization using GANs. Section 3 details the proposed method, including network architecture, image processing, and loss function. Section 4 discusses the performances of the proposed method and quantitatively compares the proposed method against the current SOTA methods using seven benchmark datasets. Finally, Section 5 concludes this work and highlights potential directions for future exploration.

## 2 Related Work

Document image binarization has advanced with the introduction of fully convolutional networks (FCNs) [21]. Tensmeyer *et al.* [44] formulated binarization as a pixel classification learning task and utilized FCNs for document image binarization. Inspired by UNet [35], Peng *et al.* [26] proposed a convolutional encoder-decoder model for document image binarization. He *et al.* [12] proposed DeepOtsu, which initially utilized convolutional neural networks (CNNs) for document image enhancement, followed by the application of Otsu’s method [25] for document image binarization. In addition, Calvo-Zaragoza and Gallego [3] employed a selective autoencoder method to parse document images, and subsequently binarizing them using global thresholding.

The introduction of GANs [9] has enabled the generation of binarized document images. Zhao *et al.* [47] formulated binarization as an image-to-image generation task, employing conditional generative adversarial networks (cGANs) to address the challenge of combining multiscale information in binarization. Souibgui *et al.* [38] introduced an effective end-to-end framework based on cGANs (named document enhancement generative adversarial network, DE-GAN) to restore degraded document images, which achieved outstanding results on the DIBCO 2013 [30], DIBCO 2017 [33], and H-DIBCO 2018 [31] datasets. Deng *et al.* [4] proposed a method employing a dual discriminator generative adversarial network (DD-GAN) with focal loss as the generator loss function.

Suh *et al.* [40] proposed a novel two-stage GAN method using six improved cycle-consistent adversarial networks (CycleGANs) [49] for document image binarization. In this method, the generator consists of UNet [35] with EfficientNet [42], while the discriminator employs Pix2Pix GAN [14]. Based on the two-stage network architecture, Ju *et al.* [16] introduced a novel three-stage GAN

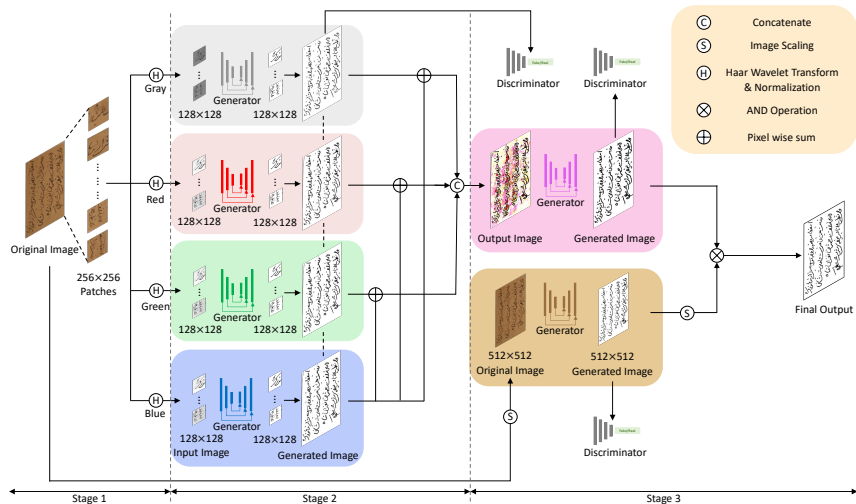


**Fig. 2:** The novel three-stage network architecture of the proposed method for document image binarization: image processing (Stage 1), document image enhancement (Stage 2), and document image binarization (Stage 3).

method, also employing six improved CycleGANs [49], with an enhanced generator using UNet++ [48] with EfficientNet [42]. Although these methods consistently outperform the SOTA performance on several DIBCO datasets, they suffer from unsatisfactory total training and inference times due to the use of multiple GANs. To address this problem, in this work, we propose a combination of image processing, generators, discriminators, and loss function components based on the network architecture of Ju *et al.* [16] to significantly reduce training and inference times.

### 3 Proposed Method

#### 3.1 Network Architecture

We employ the three-stage network architecture proposed by Ju *et al.* [16], where the overall architecture is illustrated in Fig. 2. Specifically, we use DWT and normalization to reduce the input image size in Stage 1, and propose novel generators, discriminators, and loss functions in Stages 2 and 3.

In Stage 1, the document image is divided into several patches. Unlike Ju *et al.* [16] who set the patch size to  $224 \times 224$ , we set the patch size to  $256 \times 256$ , which leads to a reduction in the number of patches obtained (i.e., by 64.3%) and hence a shorter total training time. Then we split these patches into four single-channel images (i.e., red, green, blue, and gray), because training the model on different color channels tends to generate better results. To further reduce the total training time, we apply Haar wavelet transformation [11] and normalization to reduce the patch size to  $128 \times 128$ , as detailed in Section 3.2.

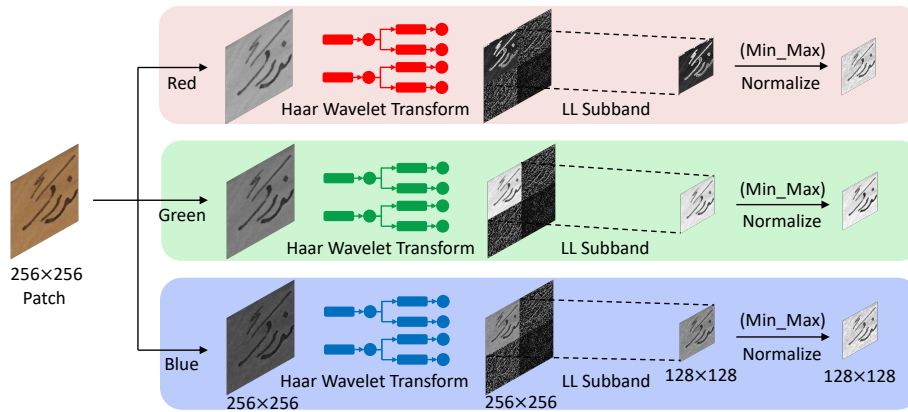


**Fig. 3:** An illustration of Stage 1 where the LL subband images of Haar Wavelet transformation are retained and normalized.

In Stage 2, we design four generators with the encoder-decoder architecture. The encoder extracts features, while the decoder performs down-sampling and extracts contextual information. Specifically, we employ UNet++ [48] with EfficientNetV2-S [43] as the generator. Each single-channel image is input to an independent generator for individual training. This method effectively removes background information from local document images and extracts detailed and colorful foreground features. To ensure the standardization of the generated images, all the images generated by the four independent generators share the same discriminator. We use the improved PatchGAN [49] as the discriminator, where we apply instance normalization to all layers except the first layer, because including instance normalization in the first layer would normalize and disregard the image color, which is not what we desired.

In Stage 3, multi-scale GANs are utilized for both local and global document image binarization to enhance the distinction between text and background. The output of Stage 2 is an image of the same size as the original input image, and it is input to an independent generator that produces the images as the result of the local document image binarization. In addition, the original input image is directly scaled to  $512 \times 512$  pixels and input into an independent generator, and the generated images are the results of global document image binarization. The generator and discriminator in Stage 3 are the same as those used in Stage 2. As shown on the right section of Fig. 2, the final output of the proposed method is the pixel-wise summation of the results from the local and global document image binarization processes.

### 3.2 Image Processing

Since the total training and inference times of the SOTA method proposed by Ju *et al.* [16] are excessively long, the primary focus and contribution of this

work is to reduce these times based on the same network architecture. It is well known that reducing the input image size can significantly decrease the model training time. However, directly reducing the input images would negatively impact the model performance. Therefore, instead of using interpolation for image size reduction, this work proposes employing DWT and normalization, because this combination of techniques can effectively preserve contour information and reduce noise interference while decreasing the image size, which is superior to the interpolation method that only considers the pixel computation. We present the related experiments in Section 4.4, which demonstrate that the global binarization results of the images processed by DWT and normalization are closer to the ground-truth images when compared to those processed by interpolation.

During image processing, DWT decomposes the input images into two components, where the low-frequency components encode the contour information, and the high-frequency components capture details and localized information. This work retains and normalizes the low-low (LL) subband images from DWT, effectively filtering out noise from document images, such as bleeding and staining. For simplicity, the Haar wavelet transformation is used as shown in Fig. 3.

### 3.3 Loss Function

Since the convergence of the loss function is unstable during the GAN training process [9], to stabilize the loss function convergence of GAN in the proposed method, we follow Suh *et al.* [40] and Ju *et al.* [16] by applying Wasserstein generative adversarial network with gradient penalty (WGAN-GP) [10] to the objective function for the model training. In addition, since the goal of document image binarization is to classify each pixel into two categories (namely, text and background), we use binary cross-entropy (BCE) Loss instead of L1 Loss employed in the original method [14, 47]. Experiments by Bartusiak *et al.* [2] demonstrated that BCE Loss outperforms L1 Loss in binary classification tasks. While BCE Loss focuses on the accuracy of each individual pixel, Dice Loss [39] emphasizes the accuracy of the entire region. Combining these two loss functions enhances the segmentation performance at both the pixel and region levels. Galdran *et al.* [7] also demonstrated that integrating BCE Loss and Dice Loss results in superior segmentation performance. Therefore, we use the improved WGAN-GP objective loss function, which includes both BCE Loss and Soft Dice Loss [22], as expressed below:

$$\mathbb{L}_G = \mathbb{E}_x[D(G(x), x)] + \lambda_1 \mathbb{L}_{BCE}(G(x), y) + \lambda_2 \mathbb{L}_{Soft\ Dice}(G(x), y), \quad (1)$$

$$\mathbb{L}_D = -\mathbb{E}_{x,y}[D(y, x)] + \mathbb{E}_x[D(G(x), x)] + \alpha \mathbb{E}_{x, \hat{y} \sim P_{\hat{y}}}[(\|\nabla_{\hat{y}} D(\hat{y}, x)\|_2 - 1)^2], \quad (2)$$

where  $x$  is the input images,  $G(x)$  is the generated images, and  $y$  is the ground-truth images.  $\lambda_1$  and  $\lambda_2$  control the relative importance of different loss terms, while  $\alpha$  denotes the gradient penalty coefficient. The discriminator  $D$  is trained to minimize  $\mathbb{L}_D$  to distinguish between ground-truth and generated images, while the generator  $G$  aims to minimize  $\mathbb{L}_G$ .

## 4 Experiments

### 4.1 Datasets

To ensure a fair comparison among the proposed method and other SOTA methods, we construct the training set following the strategy in [12, 16, 40, 45]. The training set comprises 143 images, including 10 from DIBCO 2009 [8], 10 from H-DIBCO 2010 [27], 14 from H-DIBCO 2012 [29], 7 from the Bickley Diary dataset [5], 15 from the Persian Heritage Image Binarisation Dataset (PHIBD) [1], and 87 from the Synchromedia Multispectral Ancient Document Images (SMADI) dataset [13].

We use the remaining 102 images as the testing set. The testing set consists of 16 images from DIBCO 2011 [28], 16 from DIBCO 2013 [30], 10 from H-DIBCO 2014 [24], 10 from H-DIBCO 2016 [32], 20 from DIBCO 2017 [33], 10 from H-DIBCO 2018 [31], and 20 from DIBCO 2019 [34].

### 4.2 Evaluation Metrics

To quantitatively compare the models, four classical metrics are employed: f-measure (FM), pseudo-f-measure (p-FM), peak signal-to-noise ratio (PSNR), and distance reciprocal distortion (DRD). However, when comparing the performance of different methods, there are cases where the FM and p-FM values of the model reach the SOTA level, but its PSNR value is lower than that of other methods. Therefore, to demonstrate the overall performance of each method, we adopt the Avg-Score (Avg) metric introduced by Jemni *et al.* [15]:

$$Avg = (FM + p-FM + PSNR + (100 - DRD))/4. \quad (3)$$

Note that in the Avg metric, the precision and recall metrics have a greater impact on the value than PSNR, which we consider reasonable. It is because for the method utilizing GANs to generate binarized images, the focus should be on the overall correctness of the generated image rather than the correctness of each pixel. Furthermore, as we illustrate in Section 4.7, our proposed method can generate the image more completely despite our achieved PSNR is lower than that of other methods.

### 4.3 Implementation Details

**Data Preparation** To ensure a fair comparison of performances, we utilize the same dataset and data augmentation techniques for both our proposed method and the selected benchmark methods [16, 40]. In Stage 1, the original input images are split into patches of  $256 \times 256$  size, matching the size of the images in the ImageNet [6] dataset. Data augmentation is employed to expand the training samples, with sampling scales set at 0.75, 1, 1.25, 1.5, and rotation by  $270^\circ$ , resulting in a total of 120,174 training image patches. For global document image binarization (Stage 3), the input images are directly resized to  $512 \times 512$

and subjected to horizontal and vertical flipping, as well as rotation by  $90^\circ$ ,  $180^\circ$ , and  $270^\circ$ , resulting in 804 training images.

It is noteworthy that Ju *et al.* [16] split the input images into  $224 \times 224$  sized patches in Stage 1 and subsequently applied the same data augmentation techniques to improve the model performance. This strategy increases the number of training image patches, potentially improving performance, but also significantly increasing training time. We retrain Ju *et al.*'s model by setting the patches to  $256 \times 256$ , and hence the numerical values presented in Tables 4 and 5 differ from those reported in the original paper [16].

**Pre-training** Suh *et al.*'s [40] and Ju *et al.*'s [16] methods employed EfficientNet [42] as the encoder of GANs, while ours uses EfficientNetV2 [43]. Due to constraints on data availability, all methods employ weights which are pre-trained on the ImageNet [6] dataset to enhance efficiency in model training.

**Training** To avoid influence of computing devices on the performance, all methods are trained utilizing NVIDIA RTX 4090 GPUs. All methods are implemented using Python with PyTorch being the the framework.

In Stage 2 and Stage 3, the training parameter settings are largely similar, with the only difference being the number of training epochs: 10 epochs for Stage 2, and 150 epochs for Stage 3. We choose Adam [18] optimizer to train the model, and set the initial learning rate to  $2 \times 10^{-4}$ . In addition, we configure the generator with  $\beta_1 = 0.5$  and the discriminator with  $\beta_2 = 0.999$ . More information about our implementation can be found on our GitHub page.

#### 4.4 Importance of DWT

To reduce total training and inference times, this work proposes to reduce the size of both input and corresponding ground-truth images for GANs by half. To illustrate the effectiveness of DWT and normalization in Stage 1, we consider two GAN models, namely: Model A: UNet [35] with EfficientNetV2-S [43], and Model B: UNet++ [48] with EfficientNetV2-S [43]. Table 1 records the time required for each stage, the total training and inference times of different methods. Two sets of time are recorded, i.e., "with the application of DWT and normalization in Stage 1" and "without (i.e., the *baseline* where split patches are directly supplied to the GANs)". Here, the total training time is the sum of the time required for each stage, and the total inference time is the total time taken to generate images of all the test sets. It can be seen that, for both models, the total training times are reduced when DWT and normalization are applied. Specifically, when DWT and normalization are applied, the training time reduces from 384.95h to 63.91h for Model A, and from 523.86h to 68.43h for Model B. Similarly, the total inference times are reduced from 1.12h to 0.68h for Model A, and from 1.19h to 0.77h for Model B. This demonstrates that the use of DWT and normalization can greatly reduce the total training and inference times.

We also explore other image resizing techniques, including interpolation-based algorithms such as bicubic, bilinear, area, nearest neighbor, and lanczos.



**Table 1:** Training and inference times taken by the original models before (baseline) and after apply DWT and normalization (proposed).

Method	Stage2 Train	Stage2 Predict	Stage3 Top	Stage3 Bottom	Total Train	Total Infer
UNet&V2S (Baseline)	332.28h	3.56h	47.47h	1.63h	384.95h	1.12h
UNet&V2S (DWT&Norm)	11.60h	3.45h	47.47h	1.39h	63.91h	0.68h
UNet++&V2S (Baseline)	465.28h	3.94h	52.88h	1.76h	523.86h	1.19h
UNet++&V2S (DWT&Norm)	14.12h	3.63h	49.29h	1.39h	68.43h	0.77h

**Table 2:** PSNR (dB) of the input images processed using different methods (Interpolation/DWT/DWT&Norm) for various training sets.

Method	DIBCO 2009	H-DIBCO 2010	H-DIBCO 2012	Bickley Diary	PHIBD	SMADI	Mean Values
Bicubic	71.445	72.216	71.667	64.286	69.584	69.885	69.847
Bilinear	70.940	72.164	71.460	64.065	69.711	69.859	69.700
Area	70.940	72.164	71.460	64.065	69.711	69.859	69.700
Nearest	70.954	72.038	71.591	64.199	69.689	69.827	69.716
Lanczos	71.421	72.215	71.687	64.303	69.576	69.886	69.848
DWT	62.651	67.110	59.673	53.763	58.004	59.476	60.113
DWT&Norm	71.773	72.738	72.852	64.444	70.764	69.440	70.335

We implement these techniques using the open source computer vision library (OpenCV) to downscale all  $256 \times 256$  input images and corresponding ground-truth images to  $128 \times 128$ . Furthermore, we employ the “DWT” method, and the “DWT and normalization (DWT&Norm)” method. It is noteworthy that the resized images from all these methods are not binarized, which cannot be used to calculate PSNR values directly with the corresponding ground-truth (binary) images. Therefore, we first apply global binarization to these reduced images then compute the PSNR values. We evaluate the impact of different image resizing techniques on six training sets by calculating the PSNR values (against the corresponding ground-truth images), and we compute the mean PSNR values for all images. The results are recorded in Table 2. The mean PSNR value achieved by “DWT” method is 60.113dB, indicating that images reduced directly using DWT do not have a high similarity with the corresponding ground-truth images. In addition, the mean PSNR values for resized images produced by different interpolation methods are all below 70dB. However, the mean PSNR value for images processed by DWT and normalization reaches 70.335dB, which means the images obtained by this method are closer to the corresponding ground-truth images at the pixel level. In conclusion, the results demonstrate that, the “DWT and normalization” method is more effective than other interpolation-based techniques for image size reduction for image binarization task.

**Table 3:** Comparison of performance for methods using different models to construct the generator.

Method	FM $\uparrow$	p-FM $\uparrow$	PSNR $\uparrow$	DRD $\downarrow$	Avg $\uparrow$	Total Train $\downarrow$	Total Infer $\downarrow$
UNet&B4	87.87	88.57	18.82	5.17	72.52	69.38h	0.75h
UNet&B5	88.88	89.65	18.93	4.85	73.15	81.63h	0.83h
UNet&V2S	88.83	89.87	19.07	4.86	73.23	63.91h	0.68h
UNet++&B4	89.40	90.38	19.01	4.87	73.48	85.45h	0.91h
UNet++&B5	89.76	90.75	19.15	4.51	73.79	112.74h	1.21h
UNet++&V2S	89.69	90.78	19.15	4.45	73.79	68.43h	0.77h

#### 4.5 Ablation Study

Another significant contribution of this work is the proposal of novel generators for GANs. This work aims to make the trained model generate more foreground text information by the novel generators. To demonstrate that the proposed method using UNet [35] or UNet++ [48] with EfficientNetV2 [43] is superior to the original method using UNet [35] or UNet++ [48] with EfficientNet [42], we conduct a series of experiments as shown in Table 3 to compare the model performance, total training and inference times of different generators. For the encoder of the generators, we utilize EfficientNet-B4, EfficientNet-B5, and EfficientNetV2-S.

From Table 3, it can be seen that for different encoders of GANs, the proposed methods (all models) obtain a shorter total training and inference times compared to the original methods, while achieving a higher Avg value. Specifically, the original method using UNet++ [48] with EfficientNet-B5 [42] achieves the Avg value of 73.79, with total training time of 112.74h and total inference times of 1.21h, respectively. In contrast, the proposed method obtains the same Avg value with total training time of 68.43h and total inference time of 0.77h, which represents a decrease of 39% and 36%, respectively. These experimental results demonstrate that the proposed method can greatly reduce the training and inference times while maintaining or improving the model performance.

#### 4.6 Comparison with Other Methods

We have identified the methods [37, 46] that achieve the SOTA performance on different test sets. However, these methods utilized the “leave-one-out” strategy to construct the training set, which is different from our training set described in Section 4.1. For example, when the testing set is DIBCO 2019 [34], our training sets include DIBCO 2009 [8], H-DIBCO 2010 [27], H-DIBCO 2012 [29], Bickley Diary [5], PHIBD [1], and SMADI [13] dataset. In contrast, in addition to the above datasets, the training set used by [37, 46] also includes DIBCO 2011 [28], DIBCO 2013 [30], H-DIBCO 2014 [24], H-DIBCO 2016 [32], DIBCO 2017 [33],

**Table 4:** The time taken for training and testing by the proposed and other SOTA methods for document image binarization. The shortest time and the 2nd shortest time are colored in red and blue, respectively.

Method	Model	Stage2 Train	Stage2 Predict	Stage3 Top	Stage3 Bottom	Total Train	Total Infer
Suh [40]	UNet&B4	14.73h	3.75h	65.96h	1.17h	85.61h	0.74h
Suh [40]	UNet&B5	16.30h	3.77h	282.80h	1.26h	304.12h	0.82h
Ju [16]	UNet++&B4	18.81h	3.95h	45.63h	1.29h	69.68h	0.91h
Ju [16]	UNet++&B5	21.23h	4.37h	49.23h	1.46h	76.29h	1.04h
<b>Ours</b>	UNet&V2S	11.60h	3.45h	47.47h	1.39h	63.91h	0.68h
<b>Ours</b>	UNet++&V2S	14.12h	3.63h	49.29h	1.39h	68.43h	0.77h

**Table 5:** Results achieved by the proposed and other STOA methods for document image binarization. The best performance and the 2nd best performance are colored in red and blue, respectively.

Method	Model	FM $\uparrow$	p-FM $\uparrow$	PSNR $\uparrow$	DRD $\downarrow$	Avg $\uparrow$	Total Train $\downarrow$	Total Infer $\downarrow$
Suh [40]	UNet&B4	87.95	89.01	19.10	4.83	72.81	85.61h	0.74h
Suh [40]	UNet&B5	88.56	89.90	19.31	4.46	73.33	304.12h	0.82h
Ju [16]	UNet++&B4	88.14	89.71	19.09	4.64	73.08	69.68h	0.91h
Ju [16]	UNet++&B5	89.13	90.35	19.30	4.49	73.57	76.29h	1.04h
<b>Ours</b>	UNet&V2S	88.83	89.87	19.07	4.86	73.23	63.91h	0.68h
<b>Ours</b>	UNet++&V2S	89.69	90.78	19.15	4.45	73.79	68.43h	0.77h

and H-DIBCO 2018 [31]. Therefore, it is unfair to directly compare the reported results from the aforementioned models with ours. Instead, our proposed method is only compared with SOTA methods [16, 40] that utilize the same training set.

Notably, when training models with the training set described in Section 4.1, the current SOTA results are achieved by Ju *et al.* [16]. As detailed in Section 4.3, to ensure a fair comparison of model performance, we adjust the patch size from  $224 \times 224$  to  $256 \times 256$  for this experiment. In addition, we observe that the total training time for methods using UNet [35] or UNet++ [48] with EfficientNet-B5 [42] is already longer than that of the proposed method, as shown in Table 5. Consequently, we do not further compare the methods using EfficientNet-B6 [42], as it is against the goal of reducing the total training and inference times.

#### 4.7 Experimental Results

In Sections 4.4 and 4.5, we demonstrate the impact of each improvement on the performance of the model using the three-stage network architecture proposed by

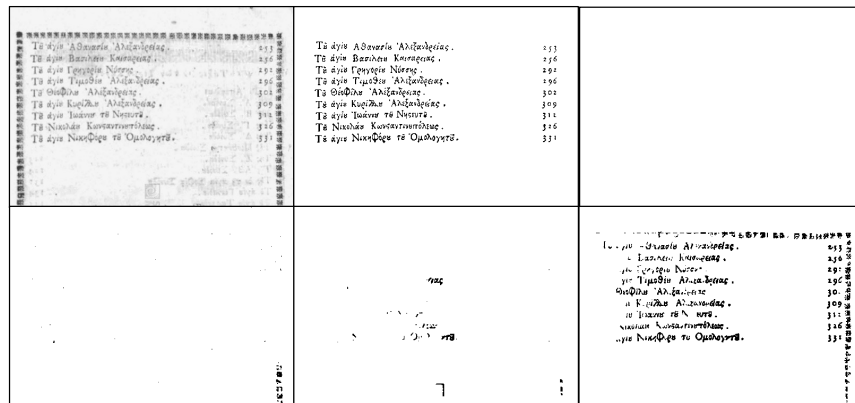
Method	Model	FM $\uparrow$	p-FM $\uparrow$	PSNR $\uparrow$
Blank Image	-	-	-	10.90
Suh <i>et al.</i> [40]	UNet&EffNet-B4	26.09	19.90	11.39
Ju <i>et al.</i> [16]	UNet&EffNet-B4	60.39	56.35	12.19
<b>Ours</b>	UNet&EffNetV2-S	69.44	69.88	11.75

**Fig. 4:** Outputs and results from document image binarization (case 1): the first row from left to right shows input image, ground-truth image, and blank image; the second row from left to right shows Suh *et al.* [40], Ju *et al.* [16], and ours.

Ju *et al.* [16]. Furthermore, we compare the proposed method with other SOTA methods on several benchmark datasets. Table 4 presents the time required for each stage, the total training and inference times for different methods. Table 5 shows the mean performance values on seven test sets: DIBCO 2011 [28], 2013 [30], 2017 [33], 2019 [34], and H-DIBCO 2014 [24], 2016 [32], and 2018 [31].

Table 4 shows that the proposed method requires less time in Stage 2, due to the reduction in the input image size for the GANs. However, compared to Ju *et al.*'s method [16], our proposed method takes longer time in Stage 3 because the newly designed discriminator has more layers. Overall, the two proposed methods achieve the shortest total training times, at 63.91h and 68.43h, respectively.

From Table 5, we can see that the proposed method using UNet++ [48] with EfficientNetV2-S [43] achieves the highest Avg value of 73.79. Our proposed method requires a total training time of 68.43h, which is much shorter than 76.29h of the method that obtains the second highest Avg value. In addition, the total inference time of our method is 0.77h, notably lower than 1.04h required by Ju *et al.*'s method [16] using UNet++ [48] with EfficientNet-B5 [42]. Next, we compare the results achieved by all the benchmark methods for each evaluation metric. Our method obtains the highest FM and p-FM values of 89.69 and 90.79, respectively, while maintaining lower total training and inference times than the method with the second highest FM and p-FM values. For the DRD metric, our



Method	Model	FM $\uparrow$	p-FM $\uparrow$	PSNR $\uparrow$
Blank Image	-	-	-	14.19
Suh <i>et al.</i> [40]	Unet&EffNet-B4	0.60	0.60	14.00
Ju <i>et al.</i> [16]	UNet&EffNet-B4	10.05	9.32	14.23
<b>Ours</b>	UNet&EffNetV2-S	56.99	56.51	14.08

**Fig. 5:** Outputs and results from document image binarization (case 2): the first row from left to right shows input image, ground-truth image, and blank image; the second row from left to right shows Suh *et al.* [40], Ju *et al.* [16], and ours.

method achieves the second highest value, but with a significantly reduced total training time of 68.43h compared to 304.12h of the method with the highest DRD value. Regarding PSNR, our method does not achieve the highest value. However, we note that the PSNR value cannot directly indicate the model’s performance, and we justify this later based on visual inspection. Overall, the aforementioned experimental results demonstrate that our method achieves the best performance on the test sets, reducing total training time by 10% and total inference time by 26% compared to the SOTA method.

We randomly select three images from the test set for visual examination and demonstrate that the PSNR value does not directly reflect the model performance. As shown in Fig. 4, our method generates more complete foreground information. However, due to the high contamination of the document image, some noise is inevitable while generating more content. In contrast, Suh *et al.*’s method [40] and Ju *et al.*’s method [16] generate little content. It should be noted that because the background is white, these methods, which generate less content, can achieve high PSNR values. In the extreme case, a completely-white image yields an a PSNR value near 11dB. These observations indicate that higher PSNR value is not indicative of better model performance. Fig. 5 reconfirms this conclusion, where a blank image yields a PSNR of 14.19dB, which is higher than that of our proposed method (14.08dB), but it is obvious that the binarized image generated by our method is closer to the ground-truth image than the

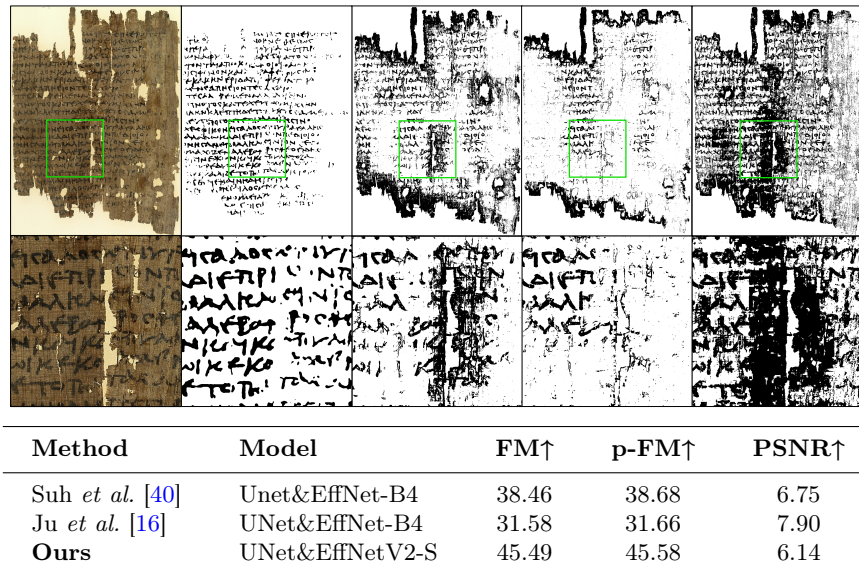


**Fig. 6:** Outputs and results from document image binarization (case 3), the first row from left to right shows input image, ground-truth image, and blank image; the second row from left to right shows Suh *et al.* [40], Ju *et al.* [16], and ours.

blank image. Fig. 6 presents another case of a lower PSNR value, where our method does not process background noise as effectively as the other two methods. Nonetheless, our method successfully generates more textual information.

## 5 Conclusion

Degraded document image binarization is an important step in document analysis. The current SOTA method utilizes a three-stage GANs architecture that can generate good document binarization results, but it suffers from long total training and inference times. To address this drawback, this work significantly improves the network based on the existing three-stage network architecture, using DWT and normalization to reduce the input image size, which greatly reduces the total training and inference times. Furthermore, novel generators, discriminators, and a loss function are designed to further improve the performance of our proposed method. Experimental results on several benchmark datasets demonstrate that the proposed method not only achieves the superior model performance but also achieves significantly shorter total training and inference times compared to the SOTA method.

As future exploration, we can combine document image binarization and document understanding for practical applications, especially for ancient or degraded documents or artifacts. The applications could include real-time translation, summarization, retrieval of related documents/materials, to name a few.

## References

1. Ayatollahi, S.M., Nafchi, H.Z.: Persian heritage image binarization competition (phibc 2012). In: International Conference on Pattern Recognition and Image Analysis (IPRIA). pp. 1–4 (2013) [7](#), [10](#)
2. Bartusiak, E.R., Yarlagadda, S.K., Güera, D., Bestagini, P., Tubaro, S., Zhu, F.M., Delp, E.J.: Splicing detection and localization in satellite imagery using conditional gans. In: IEEE Conference on Multimedia Information Processing and Retrieval (MIPR). pp. 91–96 (2019) [6](#)
3. Calvo-Zaragoza, J., Gallego, A.J.: A selectional auto-encoder approach for document image binarization. *Pattern Recognition* **86**, 37–47 (2019) [3](#)
4. De, R., Chakraborty, A., Sarkar, R.: Document image binarization using dual discriminator generative adversarial networks. *IEEE Signal Processing Letters* **27**, 1090–1094 (2020) [3](#)
5. Deng, F., Wu, Z., Lu, Z., Brown, M.S.: Binarizationshop: a user-assisted software suite for converting old documents to black-and-white. In: Joint Conference on Digital Libraries (JCDL). pp. 255–258 (2010) [7](#), [10](#)
6. Deng, J., Dong, W., Socher, R., Li, L.J., Li, K., Fei-Fei, L.: Imagenet: A large-scale hierarchical image database. In: IEEE conference on Computer Vision and Pattern Recognition (CVPR). pp. 248–255 (2009) [7](#), [8](#)
7. Galdran, A., Carneiro, G., Ballester, M.A.G.: On the optimal combination of cross-entropy and soft dice losses for lesion segmentation with out-of-distribution robustness. In: Diabetic Foot Ulcers Grand Challenge (DFUC). pp. 40–51 (2022) [6](#)
8. Gatos, B., Ntirogiannis, K., Pratikakis, I.: Icdar 2009 document image binarization contest (dibco 2009). In: International Conference on Document Analysis and Recognition (ICDAR). pp. 1375–1382 (2009) [7](#), [10](#)
9. Goodfellow, I., Pouget-Abadie, J., Mirza, M., Xu, B., Warde-Farley, D., Ozair, S., Courville, A., Bengio, Y.: Generative adversarial networks. *Communications of the ACM* **63**(11), 139–144 (2020) [2](#), [3](#), [6](#)
10. Gulrajani, I., Ahmed, F., Arjovsky, M., Dumoulin, V., Courville, A.C.: Improved training of wasserstein gans. *Advances in Neural Information Processing Systems (NeurIPS)* **30** (2017) [6](#)
11. Haar, A.: Zur theorie der orthogonalen funktionensysteme. *Mathematische Annalen* **69**, 331–371 (1910) [4](#)
12. He, S., Schomaker, L.: Deepotsu: Document enhancement and binarization using iterative deep learning. *Pattern recognition* **91**, 379–390 (2019) [2](#), [3](#), [7](#)
13. Hedjam, R., Cheriet, M.: Historical document image restoration using multispectral imaging system. *Pattern Recognition* **46**(8), 2297–2312 (2013) [1](#), [7](#), [10](#)
14. Isola, P., Zhu, J.Y., Zhou, T., Efros, A.A.: Image-to-image translation with conditional adversarial networks. In: IEEE Conference on Computer Vision and Pattern Recognition (CVPR). pp. 1125–1134 (2017) [3](#), [6](#)
15. Jemni, S.K., Souibgui, M.A., Kessentini, Y., Fornés, A.: Enhance to read better: a multi-task adversarial network for handwritten document image enhancement. *Pattern Recognition* **123**, 108370 (2022) [7](#)
16. Ju, R.Y., Lin, Y.S., Chiang, J.S., Chen, C.C., Chen, W.H., Chien, C.T.: Ccdwtgan: Generative adversarial networks based on color channel using discrete wavelet transform for document image binarization. In: Pacific Rim International Conference on Artificial Intelligence (PRICAI). pp. 186–198 (2023) [2](#), [3](#), [4](#), [5](#), [6](#), [7](#), [8](#), [11](#), [12](#), [13](#), [14](#)

17. Kang, S., Iwana, B.K., Uchida, S.: Complex image processing with less data—document image binarization by integrating multiple pre-trained u-net modules. *Pattern Recognition* **109**, 107577 (2021) [2](#)
18. Kingma, D., Ba, J.: Adam: A method for stochastic optimization. In: *International Conference on Learning Representations (ICLR)* (2015) [8](#)
19. Kligler, N., Katz, S., Tal, A.: Document enhancement using visibility detection. In: *IEEE/CVF Conference on Computer Vision and Pattern Recognition (CVPR)*. pp. 2374–2382 (2018) [1](#)
20. Kumar, A., Ghose, S., Chowdhury, P.N., Roy, P.P., Pal, U.: Udbnet: Unsupervised document binarization network via adversarial game. In: *International Conference on Pattern Recognition (ICPR)*. pp. 7817–7824 (2021) [2](#)
21. Long, J., Shelhamer, E., Darrell, T.: Fully convolutional networks for semantic segmentation. In: *IEEE conference on Computer Vision and Pattern Recognition (CVPR)*. pp. 3431–3440 (2015) [3](#)
22. Milletari, F., Navab, N., Ahmadi, S.A.: V-net: Fully convolutional neural networks for volumetric medical image segmentation. In: *International Conference on 3D Vision (3DV)*. pp. 565–571 (2016) [6](#)
23. Niblack, W.: *An introduction to digital image processing*. Strandberg Publishing Company (1985) [1](#)
24. Ntirogiannis, K., Gatos, B., Pratikakis, I.: Icfhr2014 competition on handwritten document image binarization (h-dibco 2014). In: *International Conference on Frontiers in Handwriting Recognition (ICFHR)*. pp. 809–813 (2014) [2](#), [7](#), [10](#), [12](#)
25. Otsu, N.: A threshold selection method from gray-level histograms. *IEEE transactions on systems, man, and cybernetics* **9**(1), 62–66 (1979) [1](#), [3](#)
26. Peng, X., Cao, H., Natarajan, P.: Using convolutional encoder-decoder for document image binarization. In: *International Conference on Document Analysis and Recognition (ICDAR)*. vol. 1, pp. 708–713 (2017) [3](#)
27. Pratikakis, I., Gatos, B., Ntirogiannis, K.: H-dibco 2010-handwritten document image binarization competition. In: *International Conference on Frontiers in Handwriting Recognition (ICFHR)*. pp. 727–732 (2010) [7](#), [10](#)
28. Pratikakis, I., Gatos, B., Ntirogiannis, K.: Icdar 2011 document image binarization contest (dibco 2011). In: *International Conference on Document Analysis and Recognition (ICDAR)*. pp. 1506–1510 (2011) [7](#), [10](#), [12](#)
29. Pratikakis, I., Gatos, B., Ntirogiannis, K.: Icfhr 2012 competition on handwritten document image binarization (h-dibco 2012). In: *International Conference on Frontiers in Handwriting Recognition (ICFHR)*. pp. 817–822 (2012) [7](#), [10](#)
30. Pratikakis, I., Gatos, B., Ntirogiannis, K.: Icdar 2013 document image binarization contest (dibco 2013). In: *International Conference on Document Analysis and Recognition (ICDAR)*. pp. 1471–1476 (2013) [3](#), [7](#), [10](#), [12](#)
31. Pratikakis, I., Zagori, K., Kaddas, P., Gatos, B.: Icfhr 2018 competition on handwritten document image binarization (h-dibco 2018). In: *International Conference on Frontiers in Handwriting Recognition (ICFHR)*. pp. 489–493 (2018) [2](#), [3](#), [7](#), [11](#), [12](#)
32. Pratikakis, I., Zagoris, K., Barlas, G., Gatos, B.: Icfhr2016 handwritten document image binarization contest (h-dibco 2016). In: *International Conference on Frontiers in Handwriting Recognition (ICFHR)*. pp. 619–623 (2016) [7](#), [10](#), [12](#)
33. Pratikakis, I., Zagoris, K., Barlas, G., Gatos, B.: Icdar2017 competition on document image binarization (dibco 2017). In: *International Conference on Document Analysis and Recognition (ICDAR)*. vol. 1, pp. 1395–1403 (2017) [2](#), [3](#), [7](#), [10](#), [12](#)



34. Pratikakis, I., Zagoris, K., Karagiannis, X., Tsochatzidis, L., Mondal, T., Marthot-Santaniello, I.: Icdar 2019 competition on document image binarization (dibco 2019). In: International Conference on Document Analysis and Recognition (ICDAR). pp. 1547–1556 (2019) [1](#), [7](#), [10](#), [12](#)
35. Ronneberger, O., Fischer, P., Brox, T.: U-net: Convolutional networks for biomedical image segmentation. In: International Conference on Medical Image Computing and Computer Assisted Intervention (MICCAI). pp. 234–241 (2015) [3](#), [8](#), [10](#), [11](#)
36. Sauvola, J., Pietikäinen, M.: Adaptive document image binarization. *Pattern Recognition* **33**(2), 225–236 (2000) [1](#)
37. Souibgui, M.A., Biswas, S., Jemni, S.K., Kessentini, Y., Fornés, A., Lladós, J., Pal, U.: Docentr: An end-to-end document image enhancement transformer. In: International Conference on Pattern Recognition (ICPR). pp. 1699–1705 (2022) [2](#), [10](#)
38. Souibgui, M.A., Kessentini, Y.: De-gan: A conditional generative adversarial network for document enhancement. *IEEE Transactions on Pattern Analysis and Machine Intelligence* **44**(3), 1180–1191 (2020) [2](#), [3](#)
39. Sudre, C.H., Li, W., Vercauteren, T., Ourselin, S., Jorge Cardoso, M.: Generalised dice overlap as a deep learning loss function for highly unbalanced segmentations. In: International Workshop on Deep Learning in Medical Image Analysis (DLMIA). pp. 240–248 (2017) [6](#)
40. Suh, S., Kim, J., Lukowicz, P., Lee, Y.O.: Two-stage generative adversarial networks for binarization of color document images. *Pattern Recognition* **130**, 108810 (2022) [2](#), [3](#), [6](#), [7](#), [8](#), [11](#), [12](#), [13](#), [14](#)
41. Sun, B., Li, S., Zhang, X.P., Sun, J.: Blind bleed-through removal for scanned historical document image with conditional random fields. *IEEE Transactions on Image Processing* **25**(12), 5702–5712 (2016) [1](#)
42. Tan, M., Le, Q.: Efficientnet: Rethinking model scaling for convolutional neural networks. In: International Conference on Machine Learning (ICML). pp. 6105–6114 (2019) [3](#), [4](#), [8](#), [10](#), [11](#), [12](#)
43. Tan, M., Le, Q.: Efficientnetv2: Smaller models and faster training. In: International Conference on Machine Learning (ICML). pp. 10096–10106 (2021) [5](#), [8](#), [10](#), [12](#)
44. Tensmeyer, C., Martinez, T.: Document image binarization with fully convolutional neural networks. In: International Conference on Document Analysis and Recognition (ICDAR). vol. 1, pp. 99–104 (2017) [3](#)
45. Vo, Q.N., Kim, S.H., Yang, H.J., Lee, G.: Binarization of degraded document images based on hierarchical deep supervised network. *Pattern Recognition* **74**, 568–586 (2018) [2](#), [7](#)
46. Yang, Z., Liu, B., Xiong, Y., Wu, G.: Gdb: gated convolutions-based document binarization. *Pattern Recognition* **146**, 109989 (2024) [2](#), [10](#)
47. Zhao, J., Shi, C., Jia, F., Wang, Y., Xiao, B.: Document image binarization with cascaded generators of conditional generative adversarial networks. *Pattern Recognition* **96**, 106968 (2019) [3](#), [6](#)
48. Zhou, Z., Siddiquee, M.M.R., Tajbakhsh, N., Liang, J.: Unet++: Redesigning skip connections to exploit multiscale features in image segmentation. *IEEE Transactions on Medical Imaging* **39**(6), 1856–1867 (2019) [4](#), [5](#), [8](#), [10](#), [11](#), [12](#)
49. Zhu, J.Y., Park, T., Isola, P., Efros, A.A.: Unpaired image-to-image translation using cycle-consistent adversarial networks. In: IEEE International Conference on Computer Vision (ICCV). pp. 2223–2232 (2017) [3](#), [4](#), [5](#)